

Effects of Pulsed Unipolar and Bipolar Current Regimes on the Characteristics of Micro-Arc Oxidation Coating on LZ91 Magnesium-Lithium Alloy

Shuo-Jen Lee¹, Le-Hung-Toan Do^{1,*}, Jeou-long Lee², Chang-Yong Chen³, Huan-Chih Peng¹

¹ Department of Mechanical Engineering, Yuan Ze University, Chung-Li, Taiwan 32003, R.O.C.

² Department of Chemical and Materials Engineering, Lunghwa University of Science and Technology, Guishan, Taoyuan County 33306, Taiwan, R.O.C.

³ AMLI Materials Technology Co., Ltd., No.61-1, Chang'an St., Bade Dist., Taoyuan City 33465, Taiwan, R.O.C.

*E-mail: toandlh@gmail.com, s1028705@mail.yzu.edu.tw

Received: 17 November 2017 / Accepted: 8 January 2018 / Published: 5 February 2018

Micro-arc oxidation (MAO) coatings on magnesium-lithium alloys were performed in an alkaline-silicate electrolyte using pulsed unipolar and bipolar current regimes to improve the corrosion resistance. The effects of a negative duty cycle of a pulsed bipolar current on the coating performance were studied at 10%, 20% and 30%. The surface morphology, element composition and phase composition of MAO coatings were examined by SEM, EDS and XRD, respectively. The corrosion resistance and porosity of the coatings were studied by potentiodynamic polarization which was performed in 3.5% NaCl solution at 25°C. The effects of the negative duty cycle on the MAO coating process and the resulting coating characteristics were discussed. Applying the pulsed bipolar current was found to promote a thinner compact coating. The corrosion resistance of the magnesium-lithium alloy was significantly improved after treatment with pulsed unipolar and bipolar current regimes. The results show that applying a 20% negative duty cycle in a pulsed bipolar current regime produces better corrosion resistance than 10% and 30% MAO coated samples.

Keywords: Micro-Arc Oxidation; unipolar current mode; bipolar current mode; negative duty cycle; Mg-Li alloy

1. INTRODUCTION

Magnesium alloys are the lightest of structural metals and have been utilized in various industries such as communications, automobile, aerospace, etc. They have very good properties including low density, high specific strength, high damping capacity, good electromagnetic shielding

and high recyclable ability [1-3]. However, the high susceptibility to corrosion of magnesium in aggressive environment lead to an unattractive surface appearance and decreased its mechanical stability. Therefore, the extensive application of magnesium alloys is limited [4, 5]. Magnesium alloying with lithium are known as the ultra-light weight materials and remarkably malleable. The extremely inferior corrosion resistance of Mg-Li alloy due to the ionization tendency and high chemical reactivity of lithium. Compared with common magnesium alloys, studied concerning the anti-corrosion improvement of Mg-Li alloys is still not much [6, 7]. Hence, a suitable method to delay the rate of corrosion and protect the surface of magnesium-lithium alloys is urgently necessary.

Many kind of surface modification technologies have often been applied to improve the properties of the magnesium alloys' surfaces, which include chemical conversion coatings, vapor deposition, organic coatings, electrochemical plating, anodizing and micro-arc or plasma electrolytic oxidation, etc. [8-11]. Among these technologies, the micro-arc oxidation is a popular method to be used to improve the corrosion resistance of magnesium alloys surface. Micro-arc oxidation technique is highly effective, simple operation, and environmentally friendly surface modification technology. The ceramic coating, which including thin inner barrier and porous outer layers, is fabricated on the magnesium alloys by the action of electricity in a suitable electrolyte. [12-14]. Complex phase-transformations caused by extreme pressures and temperatures evolved in the discharge channels produced a thick, compact and hard coating. This coating has high corrosion resistances and attractive abrasion [15].

Several studies have been conducted on the effect of electrical parameters, such as current regimes, current density, voltage, frequency, duty cycle, etc. on the coatings features [16-21]. Direct current (DC), alternative current (AC), pulsed unipolar (PUP) and pulsed bipolar (PBP) current regimes were applied on an MAO coating technique. The characteristics of spark discharge varied considerably with the type of current mode employed [2]. Pulsed unipolar and pulsed bipolar current regimes were reported to be successful in improving the properties and corrosion resistance of MAO coatings produced on magnesium alloys. According to Hussein *et al.* [22], the pulsed bipolar current regime was found to be more efficient than a pulsed unipolar regime. MAO coatings produced under a pulsed bipolar mode appear to have larger pores and defects due to strong spark discharges. Wang *et al.* [23] reported that coating fabricated under a bipolar current mode created a stronger protection against corrosion due to a greater thickness and denser and more homogeneous coatings. On the contrary, Gao *et al.* [19] reported that MAO coatings that were produced using the pulsed unipolar mode provided better corrosion performance than the pulsed bipolar MAO coatings. The negative biasing appeared to deteriorate the stability of the pulsed bipolar MAO coatings, whereas the pulsed unipolar mode provided conditions for stable oxide growth. Further extension of the cathodic current density beyond the critical value (20 mA.cm^{-2}) impeded the production of MAO coating due to the development of an unstable passive state on the surface. The MAO coating properties were also affected by the duty cycles of the pulsed unipolar and bipolar modes. Increasing the duty cycle refers to an increase in the application time of the current during each period. The energy density of the sparks and the amount of heat released during the process increased with the increase in the duty cycle [24, 25]. In a study by V. Dehnavi *et al.* [20], micro-discharges with a higher spatial density and a lower intensity are produced by applying low duty cycles which lead to smaller craters.

Recently, the properties of MAO coating fabricated on magnesium lithium alloys have been studied [26-29]. However, information on the role of the duty cycle of pulsed unipolar and bipolar current modes on MAO coating is limited in literature. In this paper, we aimed at understanding the effect of a negative duty cycle under a pulse-bipolar mode on the characteristics of MAO coating on a LZ91 magnesium-lithium alloy. The surface morphology, element composition, phase composition and anti-corrosion performance of the MAO coatings obtained were then analyzed by scanning electron microscopy (SEM), energy dispersive spectroscopy (EDS), X-ray diffractometry (XRD) and potentiodynamic polarization, respectively.

2. EXPERIMENT

2.1 Preparation of MAO coating

Specimens of LZ91 magnesium-lithium alloy (Mg - 9 mass% Li – 1 mass% Zn) alloy, with a sizes of 50 mm × 50 mm × 5 mm, were formed from ingots material after rolling process. Before MAO treatment, LZ91 alloy specimens were ground and polished using abrasive SiC paper up to 1500 grit to achieve a smooth surface; then, rinsed with distilled water, ultrasonically degreased in acetone for 10 min, and finally, dried in hot air.

The MAO coatings were conducted in the electrolyte containing 4 g/L sodium hydroxide (NaOH), 15 g/L sodium metasilicate (Na_2SiO_3), 5 g/L sodium phosphate tribasic dodecahydrate ($\text{Na}_3\text{PO}_4 \cdot 12\text{H}_2\text{O}$) and additives.

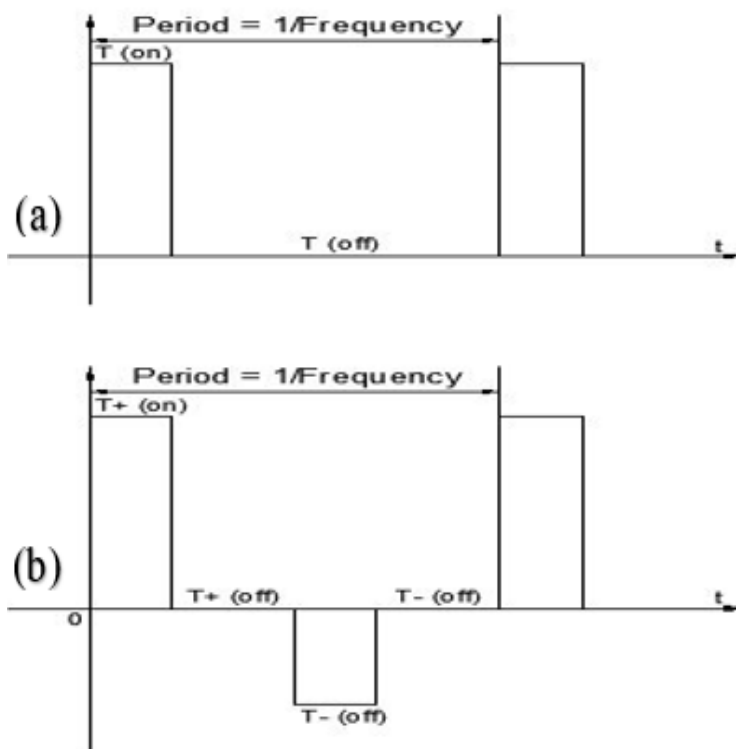


Figure 1. Schematic illustration of (a) pulsed unipolar and (b) pulsed bipolar current regimes.

A micro-arc oxidation of the specimen was carried out in an alkaline silicate electrolyte under pulsed unipolar and bipolar current modes. The substrate, which was connected to a positive output power supply, was immersed in an electrolyte acting as the working electrode and a stainless steel container, which was connected to a negative output power supply, serving as the counter electrode. Figure 1 illustrates the schematic of the pulsed unipolar and pulsed bipolar current regimes applied in this research. The positive current density and pulsing frequency were set at 4 A/dm^2 and $f = 1 / (T_{on}^+ + T_{off}^+ + T_{on} + T_{off}) = 1000 \text{ Hz}$, respectively. The duty cycle of the pulsed unipolar current mode was set at $\delta^+ = T_{on}^+ / (T_{on}^+ + T_{off}^+) = 30\%$. With a pulsed bipolar current mode, the negative current density was set at 2 A/dm^2 and the positive and negative duty cycles were set at $\delta^+ = T_{on}^+ / (T_{on}^+ + T_{off}^+ + T_{on} + T_{off}) = 30\%$ and $\delta^- = T_{on}^- / (T_{on}^+ + T_{off}^+ + T_{on} + T_{off}) = 10\%, 20\% \text{ and } 30\%$, respectively. During the MAO process, the cooling system was used to keep the temperature of the electrolyte at an ambient temperature. The MAO process was carried out for 15 min. After MAO coating, the coated samples were taken out from electrolyte, rinsed thoroughly with DI water and dried in hot air for 10 min.

2.2 Characterization of MAO coating

The thicknesses of the MAO coatings were measured using a Fischer dualscope MP20 for non-ferrous materials. The surface and cross-section morphology of the MAO coated magnesium-lithium alloy were studied by scanning electron microscope (SEM - FEI Nova NanoSEM 230). The chemical compositions of coating were studied using an energy dispersive spectroscope (EDS) incorporated with the SEM. The phase compositions were analyzed using X-ray diffractometry (XRD - X'pert Powder, PANalytical) analysis with $\text{Cu-K}\alpha$ radiation. The scanning was within $2\theta = 20^\circ - 80^\circ$, at a grazing angle of 1° .

The potentiodynamic polarization was performed to investigate corrosion resistance and measure porosity of the coatings. The electrochemical measurements were conducted on Solartron 1285 Potentiostat system in a 3.5 wt% NaCl solution at room temperature using a conventional three-electrode cell with a LZ91 substrate or MAO coated samples with an exposed area of 1 cm^2 as the working electrode, a platinum plate as the counter electrode and a silver chloride electrode (Ag/AgCl/Sat. KCl) as the reference electrode. Potentiodynamic polarization scans were performed at a sweep rate of 1 mV/s in the potential range of -1.8 V to -1.2 V vs. reference after an initial 5-minute delay. Solartron Corrware and Corrview software is used for data acquisition and plotting.

The coating porosity was measured by an electrochemical method. The fundamentals of the evaluation were based on the ratio of the current density through the pores and the coating. The cathodic currents are negligible in the determination of porosity, and the current density is inversely proportional to the polarization resistance [30]. The porosity of the ceramic coatings was evaluated using Equation (1):

$$P = \left(\frac{R_{ps}}{R_p} \right) \times 10^{\frac{-|\Delta E_{corr}|}{\beta_a}} \quad (1)$$

where P is the coating porosity and $R_{p,s}$ and β_a are the polarization resistance and anodic Tafel slope of the uncoated substrate, respectively. R_p is the polarization resistance of the MAO coated substrate, and ΔE_{corr} is the difference in corrosion potential between the uncoated and the MAO coated substrates.

3. RESULTS AND DISCUSSION

3.1 Cell voltage-time response of MAO coating process

The voltage transients during the MAO coating process were recorded every 0.01 s, while the current density was kept constant at a certain value. Figure 2 shows the voltage–time response for MAO coatings formed under a pulsed unipolar regime and pulsed bipolar regime with a 10%, 20% and 30% negative duty cycle. Judging from the voltage growth rate, the MAO process can be divided into various stages of coating formation. The cell voltage rises drastically and linearly at a very high rate in the first stage of the MAO process, which is attributed to the traditional anodization process [31]. There were only a few tiny oxygen bubbles that appeared on the sample's surface, which indicated that the substrate was dissolved and a barrier layer had formed on the surface of the magnesium–lithium alloy. The second stage started when the micro sparks were initially observed on the sample's surface. The voltage at which this occurs is termed breakdown voltage. After the breakdown voltage, the potential continued to increase at a lower rate leading to thickening of the oxide layer. The start of micro-arc oxidation is recognized by the observation of a shrill sound. The oxygen evolution became vigorous, a large number of tiny sparks randomly appeared, quickly moving over the entire surface of the sample. With the progress in time, the sparks grew in size and moved slowly across the surface of the sample. The MAO process entered the third stage when the variation in voltage with time reached a stable value. In this stage, a harsh sound was heard, the micro sparks transformed into powerful sparks and the number of sparks decreased. According to Shi *et al.* [28], the large sized pores and thermal cracking of the oxide film occurred due to the intense sparking and oxygen evolution. These reactions repeatedly occurred on the surface of the sample leading to an increase in the MAO coating thickness.

Four cases, a pulsed unipolar regime and pulsed bipolar regime with 10%, 20% and 30% negative duty cycles, have the same cell voltage-time responses. As shown in Figure 2, the breakdown voltage and the final voltage (about 416 V) of a sample treated under a pulsed unipolar regime was higher than samples treated under a pulsed bipolar regime. Figure 2 also demonstrates that the positive voltage increased as the negative duty cycle decreased. The final voltage was reduced from 389 V for the 10% negative duty cycle to 375 V and 366 V for the 20% and 30% negative duty cycles, respectively. Increasing the negative duty cycle of a pulsed bipolar regime from 10% to 30%, results in a lower final voltage which indicates a thinner MAO coating. This deduction is in accordance with the results of coating thickness measurements using the Eddy test method.

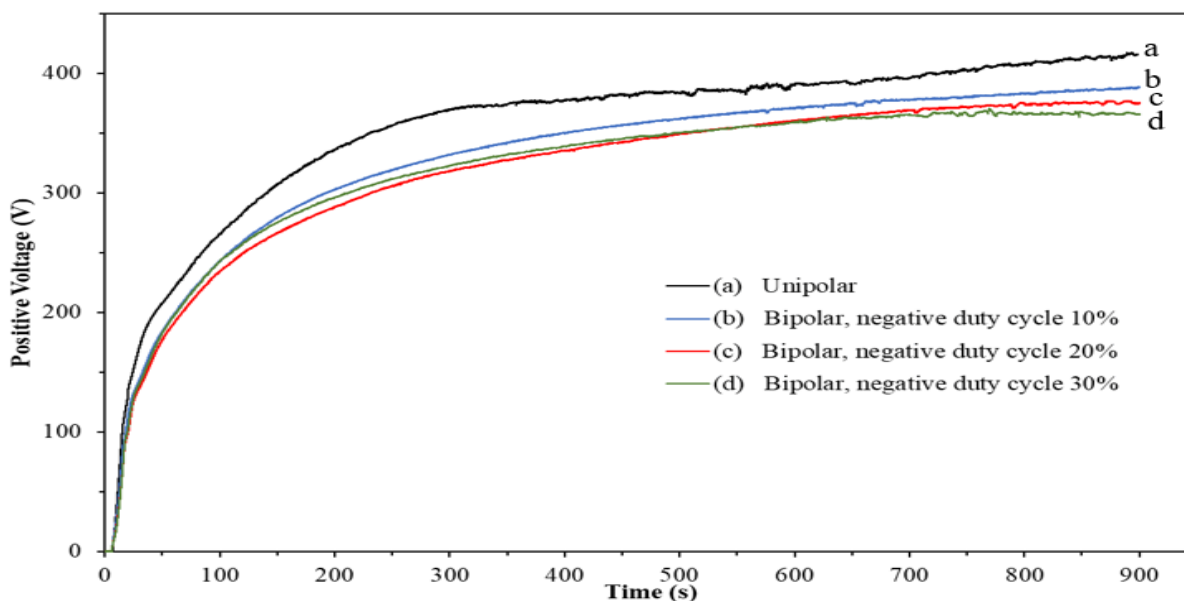


Figure 2. Cell voltage-time response for MAO coatings of LZ91 alloy produced under a pulsed unipolar regime and pulsed bipolar regime with different negative duty cycles.

3.2 MAO coating thickness

The thicknesses of the MAO coatings were obtained by averaging the results of nine measurements on the surface using the Eddy current test method. Table 1 shows the thicknesses of the MAO coating samples produced by a unipolar regime and bipolar regime with 10%, 20% and 30% negative duty cycles. According to the results in Table 1, the thicknesses of the MAO coating are significantly influenced by the current regimes and negative duty ratio. The unipolar regime produces the thickest MAO coating, at about 28.2 μm , which indicates that the growth rate is higher compared with the bipolar regime.

Table 1. Thickness of MAO coatings fabricated under a pulsed unipolar regime and pulsed bipolar regime with different negative duty cycles.

Sample ID	Average thickness (μm)	Standard deviation (μm)	Lowest value (μm)	Highest value (μm)
Unipolar	28.2	0.70	27.1	29.0
Bipolar ($\delta = 10\%$)	25.8	0.59	25.1	26.8
Bipolar ($\delta = 20\%$)	25.5	0.63	24.3	26.2
Bipolar ($\delta = 30\%$)	25.0	0.60	24.0	26.0

The coating thickness decreases with the increase in the negative duty cycle of a bipolar regime, which is a decrease from 25.8 μm at a 10% negative duty cycle to 25.5 μm at a 20% negative duty cycle and 25.0 μm at a high negative duty cycle. The results were corroborated by results obtained from the cross-sectional images (Figure 4). According to Shi *et al.* [28], the thicknesses of coatings are related to the cell voltage-time response. Thicker coatings signify a relatively higher resistance which results in a higher voltage in the later stage. Increasing the negative duty cycle decreases the standard deviation of the coating thickness. This indicates that the negative duty cycle helps the MAO coating thickness become more uniform.

3.3 Morphologies characteristics of MAO coatings

Figure 3 shows the surface morphologies of MAO coating on an LZ91 alloy under pulsed unipolar and bipolar regimes with 10%, 20% and 30% duty cycles. It can be observed that the surface of ceramic coatings formed by the MAO process have a porous microstructure, sparse cracks and some volcano top-like pores distributed disorderly, which were constituted by oxygen bubble generated on specimen and the energy through the discharge channel during MAO coating process. The pores size is obviously affected by the different current regimes. The coating formed under the pulsed unipolar regime showed a coarser structure than the coating formed under the pulsed bipolar regime. Figure 3 illustrates the effect of the negative duty cycle on the morphology of MAO coating. The coating formed under pulsed bipolar regimes with a 20% negative duty cycle showed a finer and less porous structure compared with coatings formed by 10% and 30% negative duty cycles but the difference is not very much. The size and surface features of the volcano top-like pores are reflections of the gas evolution, density and intensity of sparks during the MAO process. The more intense the sparking and gas evolution; the larger the pore size. According to Gao *et al.* [19], in the pulsed bipolar regime, the formation of smaller pores is due to the reduced discharge intensity in each cycle and/or avoidance of discharge localization at the same location. The cathodic pulse has a crucial role in promoting the soft sparking condition in the pulsed bipolar MAO process. Sah *et al.* [32] reported that the cathodic breakdown can randomize the anodic breakdown sites, thus reducing the pore diameters of the MAO coatings.

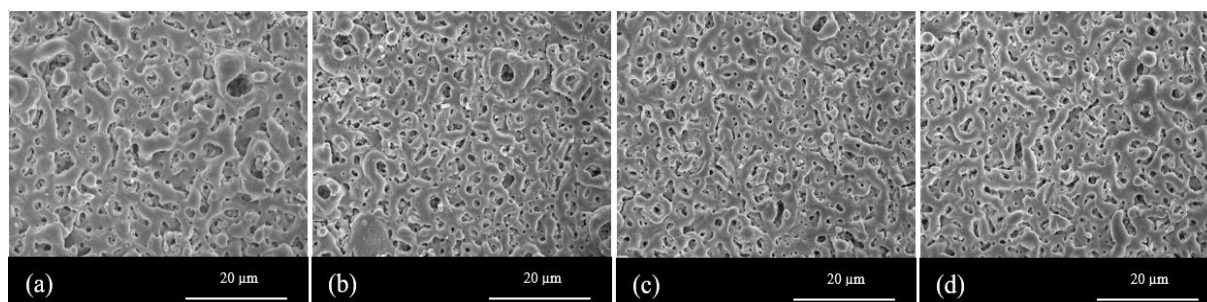


Figure 3. SEM images of top morphology of MAO coatings on LZ91 produced under (a) pulsed unipolar regime, pulsed bipolar regime with (b) 10%, (c) 20% and (d) 30% duty cycles.

Cross-sectional morphologies of the pulsed unipolar and bipolar coatings, prepared by mounting the samples into resin, are shown in Figure 4. The MAO process is composed of two different ceramic layers on magnesium alloys - an outer porous layer and a very thin inner barrier layer [33]. The cross-sectional images show that the coatings are relatively dense and compact. The coatings fabricated under a pulsed unipolar regime appear thicker compared to those fabricated under a pulsed bipolar regime. The coating thicknesses decreased with the increase in negative duty cycle. A lower negative duty cycle could provide a higher growth rate for the MAO coating. The results are consistent with results obtained from coating thickness measurements using the Eddy current test method. This decrease in coating thickness can be attributed to the lower energy input during MAO coating with the increasing negative duty cycles.

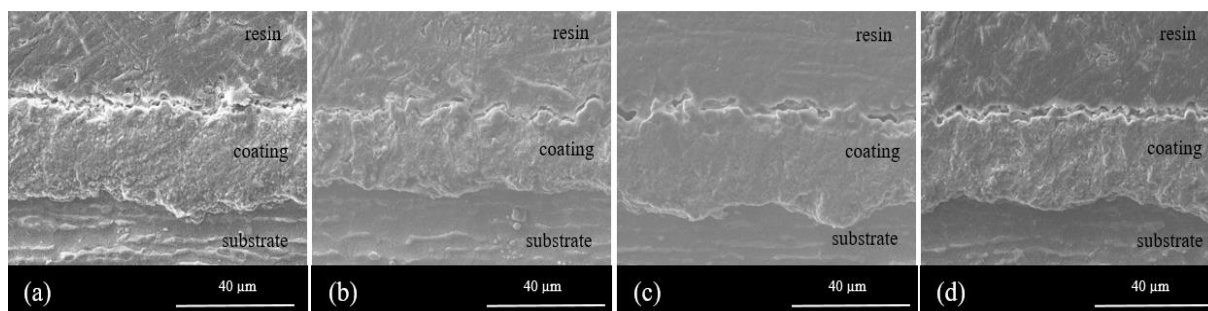


Figure 4. SEM images of cross-sectional of MAO coatings on LZ91 produced under (a) pulsed unipolar regime, pulsed bipolar regime with (b) 10%, (c) 20% and (d) 30% negative duty cycles.

3.4 Elemental and phase compositions of MAO coatings

The atomic concentrations of the elements on MAO coatings analyzed using EDS are shown in Table 2. The results indicate that all the coatings are composed of Mg, O, F, P, Na, Si and Zn. The coatings contain considerable amounts of magnesium and oxygen. The ratio of Mg/O is lower than 1, indicating that the abundance of O may be combined with other elements besides Mg, such as P, Zn and Si, in the coatings. With the increase in the negative duty cycle, the amount of F, Na and Si decreases while the amount of Mg, O and P increases. These results may be attributed to the effect of cathodic micro discharge during the micro arc oxidation process. According to Gao *et al.* [19], in the first stage of the MAO coating process, the substrate was passivated rapidly, forming an inner barrier layer. Once the voltage achieved a breakdown voltage, the discharge took place. Under the electrical field, the cations (Mg^{2+} , Zn^{2+}) from the specimen moved outwards while the anions (OH^- , O^{2-} , PO_4^{3-} , F^-) from the electrolyte were driven inwards in the discharge channels. These cations and anions combined together, resulting in the fabrication of solid compounds. These repeated reactions make the MAO coating thicker. The cathodic discharge channel attracted the cations released from the substrate under the anodic discharge channel. Therefore, the amount of Mg in the coating under a pulsed bipolar mode was higher than that under a pulsed unipolar mode. It also prevented the movement of fluoride anions to the coatings.

Table 2. Elemental composition of the coating identified by EDS (at.%).

Electrical mode	Element (at.%)							Mg/O
	Mg	O	F	P	Na	Si	Zn	
Unipolar	35.30	49.82	6.50	0.36	1.85	5.54	0.64	0.71
Bipolar ($\delta = 10\%$)	39.78	50.48	3.84	0.78	0.19	4.37	0.56	0.79
Bipolar ($\delta = 20\%$)	38.77	50.96	3.27	1.20	0.48	4.91	0.41	0.76
Bipolar ($\delta = 30\%$)	38.28	51.52	3.70	1.44	0.45	4.23	0.39	0.74

X-ray diffraction was used to indicate the phase compositions of the coatings. The XRD patterns of the oxide coatings fabricated in the variations of negative duty cycles are shown in Figure 5. The results indicate that the MAO coatings were mainly constituted with MgO and MgSiO₃, and with the additions of NaF in the electrolyte, the coatings also contained MgF₂. The results supported the findings of EDS analysis. Variation in the negative duty cycle did not result in any significant change in the phase compositions of the MAO coating formed in the same electrolyte.

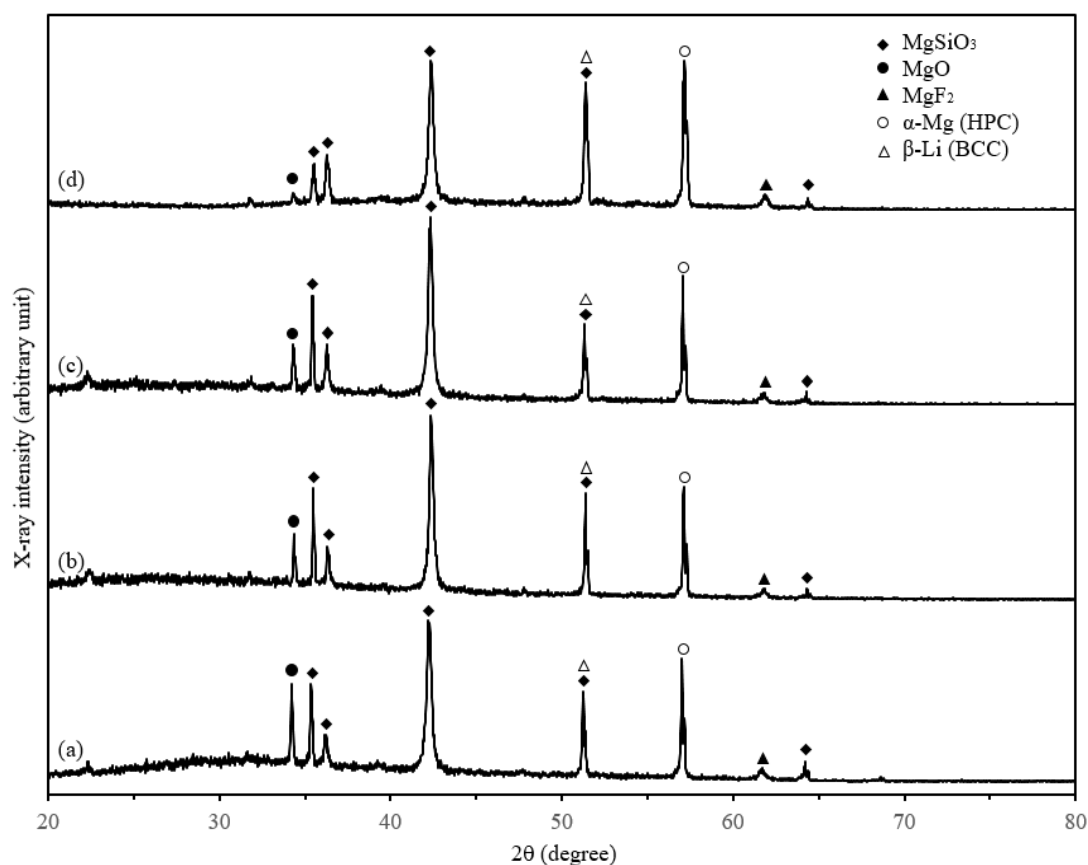


Figure 5. XRD patterns of MAO coatings fabricated under (a) unipolar regime, (b) unipolar ($\delta = 10\%$), (c) unipolar ($\delta = 20\%$), (d) unipolar ($\delta = 30\%$).

3.5 Corrosion behavior of MAO coatings

Figure 6 shows potentiodynamic polarization curves of coatings fabricated on an LZ91 alloy produced under a pulsed unipolar regime and pulsed bipolar regime with 10%, 20% and 30% negative duty cycles. In a typical polarization curve, a positive corrosion potential, lower corrosion current density and higher polarization resistance correspond with a better corrosion resistance and lower corrosion rate of coating. The corrosion current density i_{corr} , corrosion potential E_{corr} and anodic β_a , cathodic β_c Tafel slopes was estimated by Tafel region extrapolation from the potentiodynamic polarization curves. This method is preferred, due to difficulties in extrapolating the Tafel line from the anode region. The polarization resistance (R_p) can be determined by the Stern-Geary equation [34, 35]:

$$R_p = \frac{\beta_a \beta_c}{2.3 i_{corr} (\beta_a + \beta_c)} \tag{2}$$

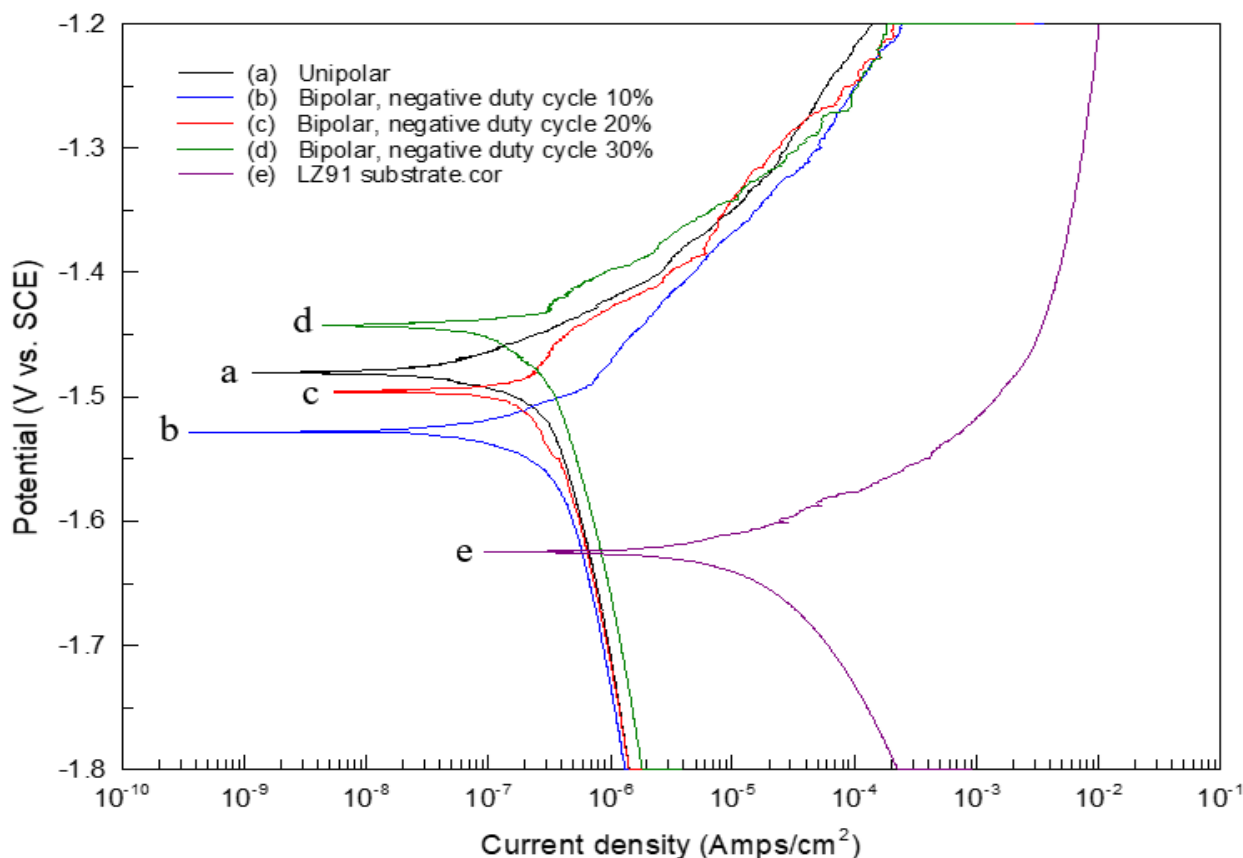


Figure 6. Potentiodynamic polarization curves of MAO coatings under (a) pulsed unipolar regime and pulsed bipolar regime with negative duty cycles of (b) 10%, (c) 20%, (d) 30% and (e) LZ91 alloy substrate.

Table 3 shows the relevant electrochemical parameters and polarization resistance calculated from the equation (2). Results show that the corrosion current density decreased from 1.36×10^{-5} A/cm² for the LZ91 alloy to 2.02×10^{-7} , 6.12×10^{-7} , 5.28×10^{-7} and 3.66×10^{-7} A/cm², and the E_{corr} shifted to a more noble direction from -1.625 V vs. Ag/AgCl for the LZ91 alloy to -1.48 V vs. SCE

for the coating under a pulsed unipolar regime and -1.528 V vs. Ag/AgCl, -1.496 V vs. SCE and -1.443 V vs. Ag/AgCl for the coatings under pulsed bipolar regimes with 10%, 20% and 30% negative duty cycles, respectively. Surface after MAO treatment illustrated superior corrosion protection properties compared with untreated LZ91 substrate. The results indicated that the anti-corrosion performance of a substrate surface had been improved significantly through the MAO process. The increase in polarization resistance, from 1.33 k Ω /cm² for an untreated LZ91 alloy to 127.67, 79.97, 88.54 and 77.17 k Ω /cm² for coatings fabricated under pulsed unipolar and pulsed bipolar regimes, also reflects the improvement in anti-corrosion performance. It can be observed that the corrosion resistance of coatings fabricated under a pulsed unipolar regime is better than for coatings fabricated under a pulsed bipolar regime. The existence of MgSiO₃ and MgF in the MAO coatings helps to protect the surface from corrosion attack as they act as physical shields between the substrate and the corrosion media. Under a pulsed bipolar regime, the coating produced with a negative duty cycle at 20% showed better polarization resistance compared with those at 10% and 30%. Duty cycle is an important electrical parameter that influences the corrosion characteristic of MAO coatings [24, 25]. Increase in negative duty cycle refers to a decrease in applied time of current during each cycle. Increase negative duty cycle decreases the energy density of the sparks, the amount of heat release during the MAO process and the amount of molten oxide that is thrown out the electrolyte. It affects to the thickness, surface morphology, phase composition and the compactness of the coatings. When applied high negative duty cycle, the thickness of MAO coating is too thin to provide effective protection to the substrate of magnesium alloy.

Table 3. Results of polarization curves analysis for MAO coatings by different negative duty cycle.

Sample ID	β_a (mV/decade)	β_c (mV/decade)	i_{corr} (A/cm ²)	E_{corr} (V vs. Ag/AgCl)	R_p (k Ω .cm ²)
Unipolar	78.0	248	2.02×10^{-7}	-1.48	127.67
Bipolar ($\delta^- = 10\%$)	127	1000	6.12×10^{-7}	-1.53	79.97
Bipolar ($\delta^- = 20\%$)	120	1020	5.28×10^{-7}	-1.50	88.54
Bipolar ($\delta^- = 30\%$)	72	665	3.66×10^{-7}	-1.44	77.17
LZ91 substrate	62	127	1.36×10^{-5}	-1.62	1.33

The porosity values of the MAO coatings were calculated using the data in Table 3. The porosities of the coatings fabricated under pulsed unipolar and pulsed bipolar regimes with negative duty cycles of 10%, 20% and 30% were 0.010 and 0.017, 0.015 and 0.017, respectively. It can be seen that the coatings fabricated under a pulsed unipolar regime are denser than those under a pulsed bipolar regime. The results support the findings obtained from the SEM micrographs. The pores on the MAO

coating act as an active area for corrosion attack. In the case of a corrosion ion incorporated into the open pores, after a certain time period it will infiltrate the poor corrosion resistance substrate, leading to the loss of protection from the MAO coating. Hence, the corrosion resistance of the MAO coating can be improved when it is thick and dense.

4. CONCLUSIONS

MAO coatings fabricated under pulsed unipolar and bipolar regimes with different negative duty cycles on an LZ91 alloy have been presented in the present work. Increasing the negative duty cycle of a pulsed bipolar regime resulted in lower final voltages, indicating a thinner and more uniform MAO coating. XRD analysis proved that the MAO coatings were mainly constituted with MgO, MgSiO₃, and MgF₂, which help to improve corrosion protection. The porosity of MAO coatings does not show significant dependence on the current regimes. The corrosion resistance of the magnesium-lithium alloy was significantly improved after being treated under pulsed unipolar and bipolar MAO coatings. The pulsed unipolar current was found to promote the best corrosion resistance coating. The 20% negative duty cycle in a pulsed bipolar current produced a better corrosion resistance than the 10% or 30% negative duty cycle.

ACKNOWLEDGMENTS

This work was accomplished with much needed support and the authors would like to thank for the financial support by Ministry of Science and Technology of R.O.C. and AmLi Co., Ltd. through the grant MOST 106-2622-E-155-001-CC2.

References

1. C. Liu, J. Liang, J. Zhou, Q. Li, Z. Peng, L. Wang, *Surf. Coat. Tech.*, 304 (2016) 179.
2. T.S.N. Sankara Narayanan, I.S. Park, M.H. Lee, *Prog. Mater. Sci.*, 60 (2014) 1.
3. M.K. Kulekci, *Int. J. Adv. Manuf. Technol.*, 39 (2008) 851.
4. J. Zhang, C. Wu, *Corros. Sci.*, 2 (2010) 55.
5. K. Ria, S.D. Choi, *J. Korean Phys. Soc.*, 54 (2009) 2409.
6. Z. Li, Y. Yuan, P. Sun, and X. Jing, *Appl. Mater. Interfaces*, 3 (2011) 3682.
7. W.R. Zhou, Y.F. Zheng, M.A. Leeflang, J. Zhou, *Acta Biomater.*, 9 (2013) 8488.
8. J.E. Gray, B. Luan, *J. Alloy. Compd.*, 336 (2002) 88–113.
9. K. Dong, Y. Song, D. Shan, E.H. Han, *Surf. Coat. Tech.*, 266 (2015) 188.
10. N. Yamauchi, N. Ueda, A. Okamoto, T. Sone, M. Tsujikawa, S. Oki, *Surf. Coat. Tech.*, 201 (2007) 4913.
11. Y. Son, D. Shan, R. Chen, F. Zhang, E.H. Han, *Surf. Coat. Tech.*, 203 (2009) 1107.
12. A. Nominé, J. Martin, G. Henrion, T. Belmonte, *Surf. Coat. Tech.*, 269 (2015) 131.
13. A. Lugovskoy, M. Zinigrad, *Materials Science - Advanced Topics, InTech*, (2013).
14. L.H. Li, T.S.N. Sankara Narayanan, Y.K. Kim, J.Y. Kang, I.S. Park, T.S. Baea and M.H. Lee, *Surf. Interface Anal.*, 46 (2014) 7.
15. R.O. Hussein, X. Nie, D.O. Northwood, A. Yerokhin and A. Matthews, *J. Phys. D Appl. Phys.*, 43 (2010) 105203.

16. X. Lu, C. Blawert, M. Mohedano, N. Scharnagl, M.L. Zheludkevich, K.U. Kainer, *Surf. Coat. Tech.*, 289 (2016) 179.
17. Z. Qiu, R. Wang, X. Wu, Y. Zhang, *Int. J. Electrochem. Sci.*, 8 (2013) 1957.
18. Y. Yue, W. Hua, *T. Nonferr. Metal. Soc.*, 20 (2010) 688.
19. Y. Gao, A. Yerokhin, A. Matthews, *Appl. Surf. Sci.*, 316 (2014) 558.
20. V. Dehnavi, B.L. Luan, D.W. Shoesmith, X.Y. Liu, S. Rohani, *Surf. Coat. Tech.*, 226 (2013) 100.
21. R.O. Hussein, D.O. Northwood, X. Nie, *Surf. Coat. Tech.*, 237 (2013) 357.
22. R.O. Hussein, P. Zhang, X. Nie, Y. Xia, D.O. Northwood, *Surf. Coat. Tech.*, 206 (2011) 1990.
23. S. Wang, Y. Xia, L. Liu, N. Si, *Ceram. Int.*, 40 (2014) 93.
24. Y. Tang, X. Zhao, K. Jiang, J. Chen, Y. Zuo, *Surf. Coat. Tech.*, 205 (2010) 1789.
25. X. Wang, L. Zhu, W. Li, H. Liu, Y. Li, *Appl. Surf. Sci.*, 255 (2009) 5721.
26. S.J. Lee, L.H.T Do, *Surf. Coat. Tech.*, 307 (2016) 781.
27. L. Song, Y. Kou, Y. Song, D. Shan, G. Zhu and E.H. Han, *Mater. Corros.*, 62 (2011) 1124.
28. L. Shi, Y. Xu, K. Li, Y. Yao, S. Wu, *Curr. Appl. Phys.*, 10 (2010) 719.
29. Z.J. Li, Y. Yuan and X.Y. Jing, *Mater. Corros.*, 65 (2014) 493.
30. C. Liu, Q. Bi, A. Leyland, A. Matthews, *Corros. Sci.*, 45 (2003) 1257.
31. S. Verdier, . M. Boinet, S. Maximovitch, F. Dalard, *Corros. Sci.*, 47 (2005) 1429.
32. S.P. Sah, E. Tsuji, Y. Aoki, H. Habazaki, *Corros. Sci.*, 55 (2012) 90.
33. D.Y. Hwang, J.Y. Cho, D.H. Lee, B.Y. Yoo and D.H. Shin, *Mater. Trans.*, 49 (2008) 1600.
34. C. Cui, *Corros. Sci.*, 52 (2010) 2228.
35. C. Wang, B. Jiang, M. Liu, Y. Ge, *J. Alloy. Compd.*, 621 (2015) 53.

© 2018 The Authors. Published by ESG (www.electrochemsci.org). This article is an open access article distributed under the terms and conditions of the Creative Commons Attribution license (<http://creativecommons.org/licenses/by/4.0/>).